

Washington University School of Medicine

Digital Commons@Becker

Open Access Publications

5-16-2021

A genetic screen for regulators of muscle morphogenesis in *Drosophila*

Tiffany Ou

Gary Huang

Beth Wilson

Paul Gontarz

James B Skeath


See next page for additional authors

Follow this and additional works at: https://digitalcommons.wustl.edu/open_access_pubs

Authors

Tiffany Ou, Gary Huang, Beth Wilson, Paul Gontarz, James B Skeath, and Aaron N Johnson

A genetic screen for regulators of muscle morphogenesis in *Drosophila*

Tiffany Ou,¹ Gary Huang,^{1,†} Beth Wilson,² Paul Gontarz ,¹ James B. Skeath,² and Aaron N. Johnson  ^{1,*}

¹Department of Developmental Biology, Washington University School of Medicine, St. Louis, MO 63110, USA and

²Department of Genetics, Washington University School of Medicine, St. Louis, MO 63110, USA

*Corresponding author: Email: anjohnson@wustl.edu

[†]Present address: Graduate Program in Genetics and Genomics, Baylor College of Medicine, Houston, TX 77030, USA.

Abstract

The mechanisms that determine the final topology of skeletal muscles remain largely unknown. We have been developing *Drosophila* body wall musculature as a model to identify and characterize the pathways that control muscle size, shape, and orientation during embryogenesis. Our working model argues muscle morphogenesis is regulated by (1) extracellular guidance cues that direct muscle cells toward muscle attachment sites, and (2) contact-dependent interactions between muscles and tendon cells. While we have identified several pathways that regulate muscle morphogenesis, our understanding is far from complete. Here, we report the results of a recent EMS-based forward genetic screen that identified a myriad of loci not previously associated with muscle morphogenesis. We recovered new alleles of known muscle morphogenesis genes, including *back seat driver*, *kon-tiki*, *thisbe*, and *tumbleweed*, arguing our screen had the depth and precision to uncover myogenic genes. We also identified new alleles of *spalt-major*, *barren*, and *patched* that presumably disrupt independent muscle morphogenesis pathways. Equally as important, our screen shows that at least 11 morphogenetic loci remain to be mapped and characterized. Our screen has developed exciting new tools to study muscle morphogenesis, which may provide future insights into the mechanisms that regulate skeletal muscle topology.

Keywords: *Drosophila*; myogenesis; *salm*; *bsd*; myotube guidance

Introduction

The mechanisms that regulate skeletal muscle morphogenesis have been remarkably understudied across Metazoa. Body wall muscles in the *Drosophila* embryo form a stereotyped pattern with 30 distinct muscles arranged in a spectacular compilation of longitudinal, acute, and oblique orientations. Remarkably, the final muscle pattern shows great diversity along the dorsal-ventral axis, but the pattern is invariant from segment to segment along the anterior-posterior axis (Bate 1990). A single embryonic segment must therefore house the essential morphogenetic information required to orchestrate the unique arrangement and functional morphogenesis of 30 individual muscles.

Mesodermal muscle precursors, known as myotubes, extend asymmetrical, amoeboid projections that navigate across the embryonic segment to contact pre-determined muscle attachment sites on ectodermal tendon precursors at the segment border. The mesenchymal myotube then establishes a myotendinous junction, regains symmetry, and acquires its final, functional orientation (Figure 1, A and B). Myotube guidance refers to the combined cellular processes of leading edge navigation and attachment site selection.

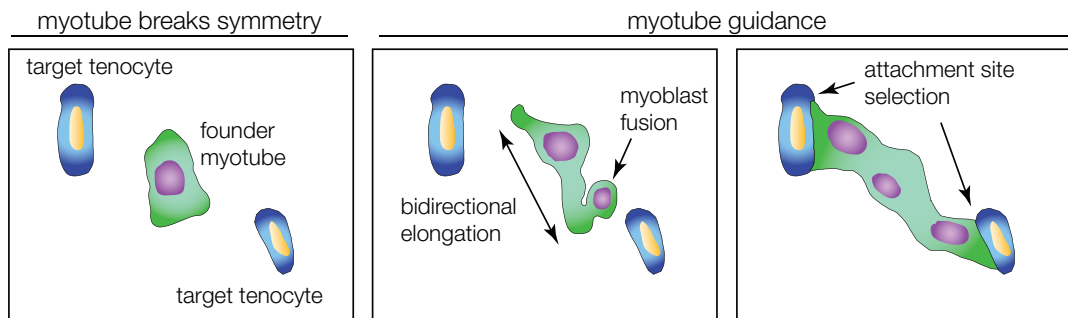
During myotube guidance, morphogenetic information is transmitted to the muscle precursors through a bipartite system (Yang et al. 2020b). Short-range secreted signals from the ectoderm provide navigational cues, which direct membrane projections toward specific muscle attachment sites. After the projections arrive at the segment border, a second type of morphogenetic information, which is presumed to reside in the tendon precursors, ensures the myotube selects the correct muscle attachment site. Incredibly, this bipartite information system ensures that individual cells from two distinct deterministic cell populations, which are specified in separate germ layers, locate one another with high fidelity during embryogenesis.

Our previous studies suggested key molecules that provide or interpret morphogenetic information during myotube guidance remain to be discovered, so we screened for novel regulators of muscle morphogenesis. To extend previous muscle screens (Chen et al. 2008; Johnson et al. 2013), we used the shape and orientation of just 5 of the 30 muscles per segment to identify and classify muscle phenotypes at single cell resolution. By focusing on a subset of muscles, we successfully obtained new alleles in 25 genes that were not previously known to regulate embryonic muscle morphogenesis

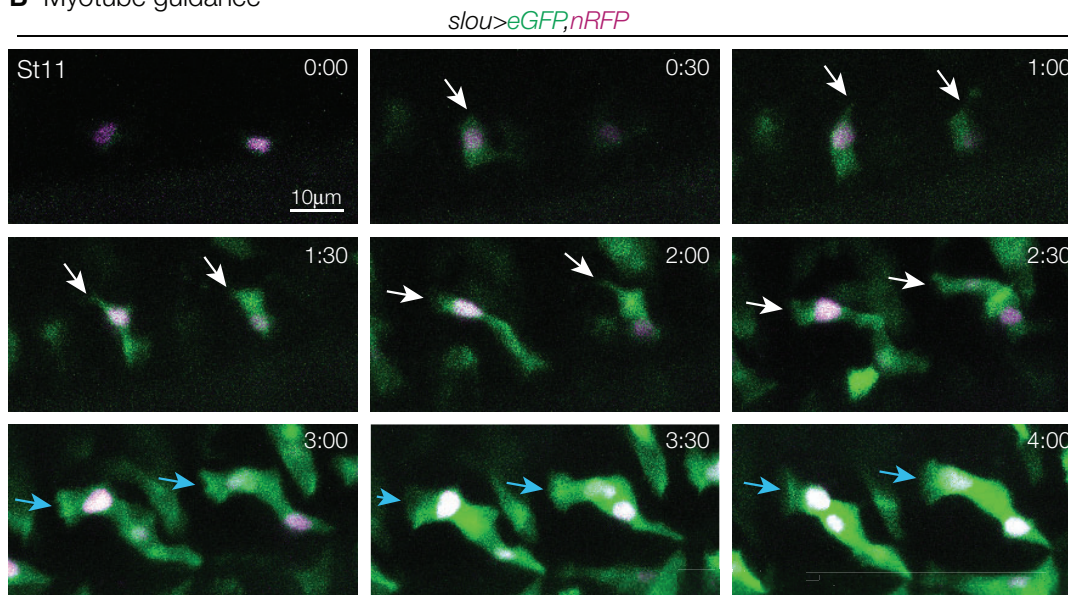
Received: March 02, 2021. Accepted: May 03, 2021

Published by Oxford University Press on behalf of Genetics Society of America 2021. This work is written by a US Government employee and is in the public domain in the US.

A Musculoskeletal system morphogenesis



B Myotube guidance



C Screen for regulators of muscle morphogenesis

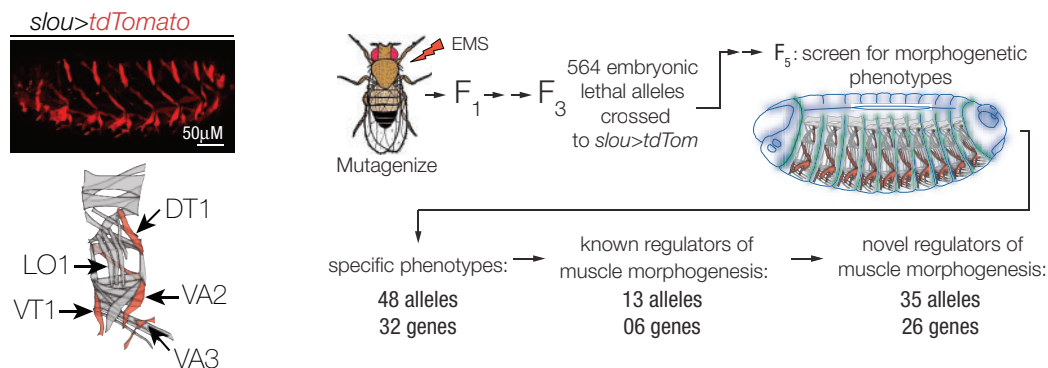


Figure 1 A genetic screen for regulators of muscle morphogenesis. (A) Diagram of *Drosophila* embryonic body wall muscle development. (Left) After cell fate specification, founder myoblasts break symmetry and become founder myotubes. (Right) Myotube leading edges elongate toward tenocytes (tendon precursors) that house the muscle attachment sites. Fusion competent myoblasts will fuse with founder myotubes during elongation. Each myotube leading edge ultimately selects the correct muscle attachment site. Myotube guidance encompasses both leading edge extension/navigation and attachment site selection. (B) Live imaging of myotube guidance. Two founder LO1 myotubes in neighboring segments expressed cytoplasmic eGFP (green) and nuclear RFP (violet) under the control of *slou*. Gal4. Arrows point to myotube leading edges during elongation (white) and during attachment site selection (blue). (###) hr: min. (C) Screening strategy. EMS-induced embryonic lethal alleles were identified and crossed with *slou>tdTomato* to visualize the morphology of the longitudinal oblique 1 (LO1), dorsal transverse 1 (DT1), ventral transverse 1 (VT1), ventral acute 2 (VA2), and ventral acute 3 (VA3) muscles in homozygous mutant embryos.

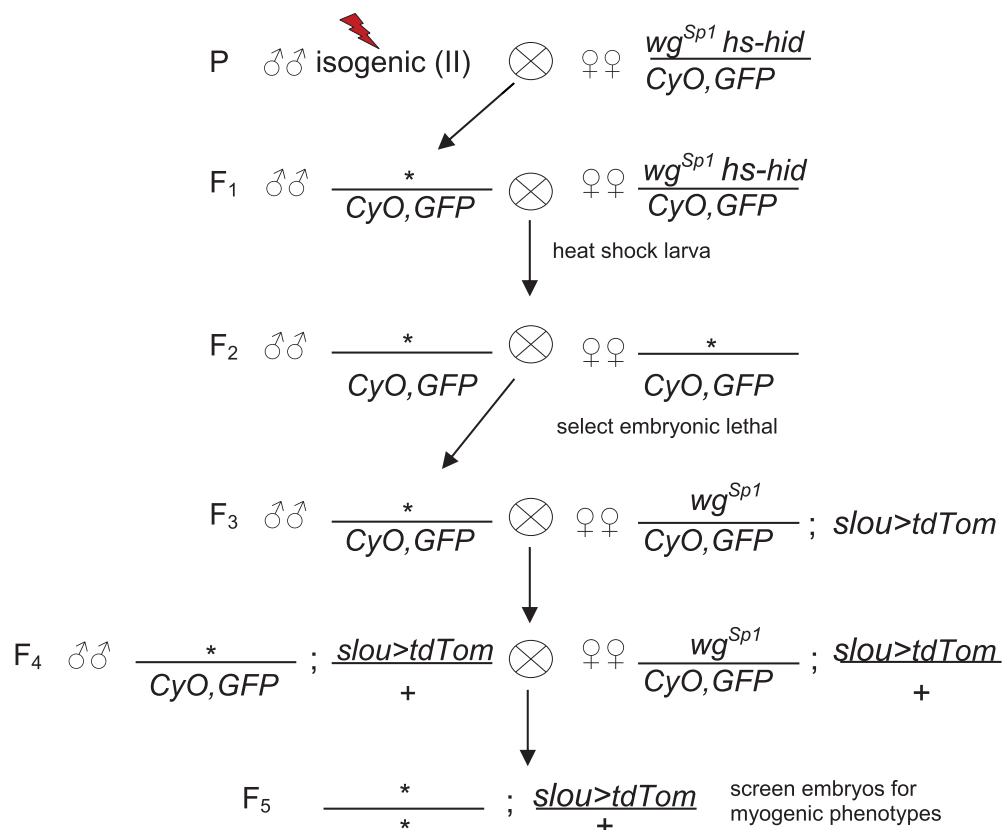
(Figure 1C). We mapped 8 alleles to causative point mutations in 4 distinct loci that encode the zinc-finger transcription factor Spalt major (Salm), the chromatin binding protein Barren (Barr), the Hedgehog (Hh) signaling regulator Patched (Ptc), and

the serine/threonine (ser/thr) kinase back seat driver (bsd). The reagents generated from this screen will provide novel inroads toward understanding the molecular mechanisms that direct muscle morphogenesis and myotube guidance.

Materials and methods

Primary screen

To generate screening stocks, flies were isogenized on chromosome II and males were treated with 25 mM EMS, which should induce approximately 3 lethal mutations per second chromosome (Asburner et al. 2005). Mutagenized males were bred as shown:



The breeding scheme utilizes two dominant markers on the second chromosome (wg^{Sp1} and CyO), which were used to follow the mutagenized chromosome (marked by “*”) through the generations. $hs-hid$ is a dominant lethal transgene. Larva were heat shocked for 1 hour a day for 3 consecutive days as indicated to remove unwanted F₂ larva with the $wg^{Sp1} hs-hid$ chromosome from the breeding scheme.

For the primary screen, 0–24 hours F₅ embryos were collected on grape plates, dechorionated, transferred to microscope slides, and $slou>tdTom$ expressing muscles were imaged in live embryos. $slou>tdTom$ is visible in 5 distinct muscles per segment (Figure 1C). The presence and morphology of individual $slou>tdTom$ muscles were used to assign mutations to phenotypic classes (see Table 1). At least 5 homozygous embryos were scored per line. The myogenic phenotypes were scored as completely penetrant, in which every embryo showed the phenotype in a majority of hemisegments, or incompletely penetrant, in which only a subset of embryos showed a phenotype in a subset of hemisegments. In total 58 lines with myogenic phenotypes were recovered from the primary screen.

Allele nomenclature

At the conclusion of the primary screen, each line was assigned a unique allele identifier $sj####$. For mapped alleles, the unique

identifier is superscripted with the gene symbol (e.g., $salm^{sj154}$). Unmapped alleles are referenced by the unique allele identifier in figures and tables (e.g., $sj168$).

Complementation analysis

The 58 lines with muscle phenotypes were inter-crossed, and transheterozygote adult viability was used for initial

complementation analysis. Because the expected background mutation rate was greater than one, the lines that failed to complement adult viability were further analyzed for transheterozygous embryonic phenotypes to confirm the noncomplementing alleles disrupted myogenesis.

The 58 lines with muscle phenotypes were also crossed to lethal alleles of known regulators of muscle morphogenesis on chromosome II, or to deficiencies that uncovered known regulators if lethal alleles were not publicly available. Screen lines that failed to complement adult viability were further analyzed for transheterozygous embryonic phenotypes. Only those lines that failed to complement embryonic phenotypes were classified as allelic to known regulators of muscle morphogenesis (see Table 2).

Stocks for complementation analysis included bsd^1 (Yang et al. 2020a), $hoip^1$ (Johnson et al. 2013), kon^{2986} (Johnson et al. 2013), $Df(2R)pyr36$ (Kadam et al. 2009), $Df(2R)ths238$ (Kadam et al. 2009), arr^2 , ban^{L305} , $Df(2R)Egfr5$, $Df(2L)BSC354 [eya]$, ptc^{tuf-D} , $Rca1^2$, $robo^1$, S^{IIIN} , $Sin3a^{e64}$, Sli^2 , smo^3 , $Df(2R)BSC269 [sns]$, tsh^{04319} , tum^{DH15} , and zip^1 . Stocks were obtained from the Bloomington Stock Center unless otherwise referenced.

Additional Drosophila stocks

Muscle morphology was visualized with $P\{GMR40D04-GAL4\}attP2$ ($slou.Gal4$), $P\{UAS-tdTom\}$, and $P\{UAS-eGFP\}$. Myoblast fusion was

Table 1 Phenotypic classes of myogenic alleles

Allele	Primary phenotype ^a	Secondary phenotype ^a
<i>bar</i> ^{sj266}	Morphogenesis-5 muscles (C)	—
<i>barr</i> ^{sj440}	Morphogenesis-5 muscles (C)	Thin muscles (C)
<i>bsd</i> ^{sj286}	Morphogenesis-5 muscles (C)	—
<i>bsd</i> ^{sj362}	Morphogenesis-5 muscles (C)	—
<i>kon</i> ^{sj204}	Morphogenesis-5 muscles (I)	—
<i>kon</i> ^{sj525}	Morphogenesis-5 muscles (C)	—
<i>ptc</i> ^{sj287}	Morphogenesis-5 muscles (C)	Oversized muscles (C)
<i>ptc</i> ^{sj461}	Morphogenesis-5 muscles (C)	Oversized muscles (C)
<i>tum</i> ^{sj316}	Morphogenesis-5 muscles (I)	—
<i>sj168</i>	Morphogenesis-5 muscles (C)	—
<i>sj245</i>	Morphogenesis-5 muscles (I)	—
<i>sj246</i>	Morphogenesis-5 muscles (I)	—
<i>sj264</i>	Morphogenesis-5 muscles (C)	—
<i>sj356</i>	Morphogenesis-5 muscles (I)	—
<i>salm</i> ^{sj154}	LO1 elongation and attachment (C)	DT1 elongation (C)
<i>salm</i> ^{sj340}	LO1 DT1 elongation and attachment (C)	VA2, VA3 elongation and attachment (I)
<i>sj9</i>	LO1 elongation and attachment (I)	—
<i>sj62</i>	LO1 attachment (I)	—
<i>sj81</i>	LO1 DT1 elongation and attachment (I)	—
<i>sj53</i>	VA2, VA3 elongation and branching (C)	—
<i>sj109</i>	VA2/VA3 branching	DT1 missing or short (I)
<i>sj130</i>	VA3 elongation (C)	—
<i>sj194</i>	VA2, VA3 elongation and branching (I)	—
<i>sj455</i>	VA3 branching (I)	—
<i>sj160</i>	VA3 elongation (I)	LO1 VA2 elongation (I)
<i>sj146</i>	LO1, VA2, VA3 elongation and attachment (I)	—
<i>sj185</i>	LO1, VA2, VA3 elongation and attachment (I)	—
<i>sj189</i>	LO1, VA3 elongation and attachment (I)	LO1 elongation and attachment (I)
<i>sj203</i>	VA2 elongation and branching (C)	LO1 elongation and attachment (I)
	VA3 missing (C)	—
<i>sj214</i>	LO1, VA1, VA3 elongation and attachment (I)	—
<i>sj237</i>	VA2 elongation and attachment (I)	LO1 elongation and attachment (I)
		DT1 missing (I)
<i>sj238</i>	LO1 VA3 elongation and attachment (I)	—
<i>kon</i> ^{sj11}	Missing DT1 LO1 VA3 (I)	—
<i>ths</i> ^{sj102}	Missing VA1 VA3 (C)	LO1 elongation and attachment (I)
<i>sj103</i>	Missing VA2 (C)	—
<i>sj348</i>	Missing VA2 (I)	LO1 VA3 elongation and attachment (I)
<i>sj278</i>	Missing VA3 (C)	VA2 elongation and attachment (C)
<i>sj371</i>	Missing VA2 VA3 (C)	LO1 elongation and attachment (I)
<i>sj405</i>	Missing DT1 VA2 VA3 (C)	—
<i>sj425</i>	Missing VA2 VA3 (C)	LO1 elongation and attachment (I)
<i>sj15</i>	Thin muscles (C)	—
<i>sj302</i>	Thin muscles (C)	—
<i>sj314</i>	Thin muscles (C)	—
<i>sj326</i>	Thin muscles (I)	—
<i>sj359</i>	Thin muscles (C)	—

^a Only DT1, LO1, and VA1-3 muscles were analyzed.

(C) Complete penetrance: all hemisegments in every embryo imaged showed the phenotype.

(I) Incomplete penetrance: a subset of embryos showed a phenotype with a subset of hemisegments affected.

assayed with $P\{kirre^{P298}.lacZ\}$ (Nose et al. 1998). *Df(2R)Exel7098* was used for complementation analysis of putative *ptc* alleles. $Cyo, P\{Gal4-Twi\}, P\{2X-UAS.eGFP\}$ was used to genotype embryos for screening, histology, and nucleic acid collection.

Allele sequencing

For RNA deep sequencing (RNAseq), total RNA was collected from 7 to 12 hours embryos per manufacturer's specification (RNeasy kit, Qiagen), and submitted to Novogene (Sacramento, CA) for deep sequencing. cDNA libraries were prepped and sequenced using 150 bp paired-end reads on the Illumina NovaSeq 6000 system. Two biological replicates were prepared and sequenced for 6 independent lines. Raw reads were quality and adapter trimmed using cutadapt (v2.4) as described (Martin 2011). Trimmed reads were aligned using STAR (v2.5.4b) to the *Drosophila* reference genome BDGP6 with Ensemble Gene

Annotation (v95) (Dobin et al. 2013). Variants for each line were called using aligned reads with the bcftools (v1.9) mpileup function followed by the bcftools call function (Li 2011). Low-quality variants were filtered using bcftools filter. Variants not found in both replicates from a line were discarded. Variants present in any complementary lines were discarded. Remaining variants were mapped to genes and prioritized using VEP (ensembl.org/Tools/VEP) (McLaren et al. 2016). RNAseq data and analysis are available at the Gene Expression Omnibus, accession number GSE164398. Causative variants were confirmed by complementation analysis with known alleles.

For Sanger sequencing, genomic DNA was collected from homozygous mutant 12–24 hours embryos using the Quick Fly Genomic DNA prep method (BDGP). Overlapping PCR amplicons were generated across the coding sequences, and TOPO cloned into PCR2.1 (ThermoFisher). M13R and T7 primers were used to

Table 2 Complementation groups with multiple alleles

Allele	Phenotype ^a
<i>bar</i> ^{sj266}	Morphogenesis-5 muscles
<i>barr</i> ^{sj440}	Morphogenesis-5 muscles, thin muscles
<i>bsd</i> ^{sj286}	Morphogenesis-5 muscles
<i>bsd</i> ^{sj348}	VA2 missing
<i>bsd</i> ^{sj362}	Morphogenesis-5 muscles
<i>kon</i> ^{sj11}	DT1 LO1 VA3 missing
<i>kon</i> ^{sj204}	Morphogenesis-5 muscles
<i>kon</i> ^{sj525}	Morphogenesis-5 muscles
<i>ptc</i> ^{sj287}	Morphogenesis-5 muscles, oversized
<i>ptc</i> ^{sj461}	Morphogenesis-5 muscles, oversized
<i>salm</i> ^{sj154}	LO1 elongation and attachment
<i>salm</i> ^{sj340}	LO1 DT1 elongation and attachment
<i>sns</i> ^{sj302}	Morphogenesis-5 muscles, thin muscles
<i>sns</i> ^{sj359}	Morphogenesis-5 muscles, thin muscles
<i>ths</i> ^{sj102}	VA1 VA3 missing
<i>ths</i> ^{sj237}	VA2 elongation and attachment
<i>sj109</i>	Morphogenesis-5 muscles
<i>sj245</i>	Morphogenesis-5 muscles
<i>sj189</i>	VA3 elongation and attachment
<i>sj203</i>	VA2 elongation and branching, VA3 missing
<i>sj278</i>	VA3 missing
<i>sj264</i>	Morphogenesis-5 muscles
<i>sj455</i>	VA3 branching
<i>sj326</i>	Thin muscles
<i>sj461</i>	Thin muscles

^a Only DT1, LO1, and VA1-3 muscles were analyzed. Complementation groups with 2–3 alleles are shown. Thirty-three single-allele complementation groups were also recovered.

sequence inserts from both the 5' and 3' ends. Point mutations were validated by sequencing multiple PCR products.

Immunohistochemistry and imaging

α - β gal (1:100, Promega, Z3781) was used to visualize rP298.lacZ. Embryo antibody staining was performed as described (Johnson et al. 2013); primary antibodies were detected with HRP-conjugated secondary antibodies and the TSA system (Molecular Probes). Embryos from the primary screen were live imaged on an Axio Observer 5 compound fluorescent microscope; follow-up imaging was used a Zeiss LSM800 confocal microscope. Imaging parameters were maintained between genotypes where possible.

Data availability

All data necessary for confirming the conclusions of this article are represented fully within the article and its tables and figures. All fly stocks are available upon request.

Results and discussion

An invariant number of mesodermal founder myoblasts and ectodermal tendon precursors (tenocytes) are specified in each abdominal segment (A2–A8) of the *Drosophila* embryo (Frommer et al. 1996; de Jossineau et al. 2012). By the end of myogenesis, the two deterministic cell populations (myoblasts and tendon cells) interact with a precise spatiotemporal stoichiometry, ostensibly through the process of myotube guidance (Figure 1, A and B) (Yang et al. 2020b). To develop new tools to study myotube guidance, we screened 564 EMS-induced lethal alleles on chromosome II for embryonic muscle phenotypes (Figure 1C). Thirty distinct muscles develop in embryonic hemisegments A2–A8, and each muscle has a unique position and morphology (Figure 1C). We visualized muscle morphology in live homozygous

mutant embryos with *slou>tdTomato*, which is expressed in the founder myoblasts that give rise to the Longitudinal Oblique 1 (LO1), Dorsal Transverse 1 (DT1), Ventral Transverse 1 (VT1), Ventral Acute 2 (VA2), and Ventral Acute 3 (VA3) muscles. In total, our screen identified 58 alleles that disrupt muscle morphogenesis.

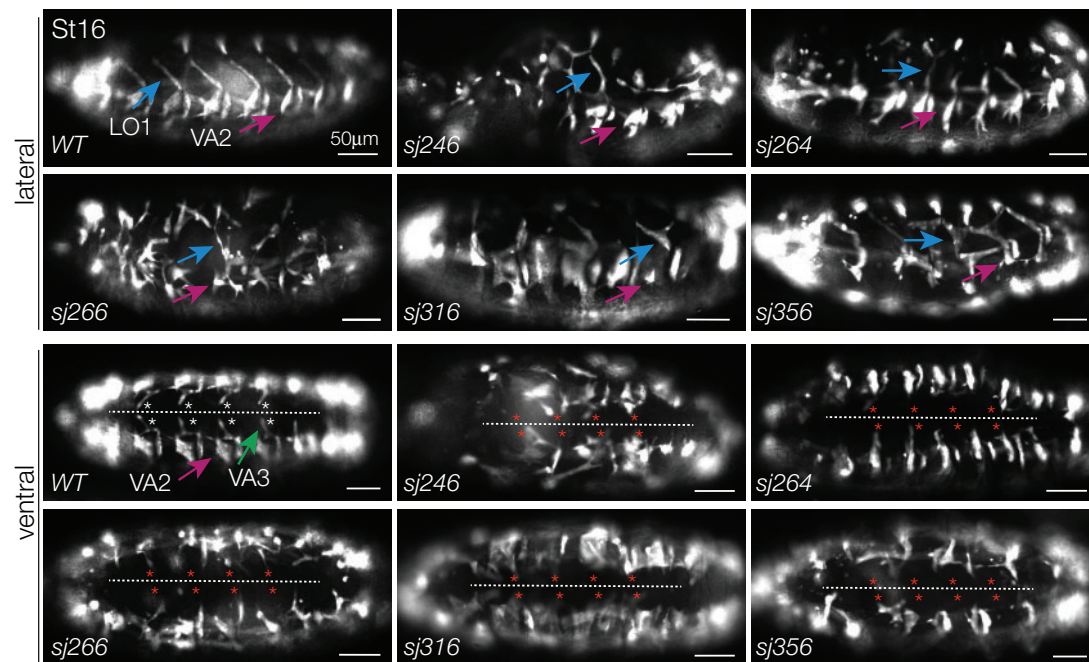
The orientation of each muscle is defined as acute, oblique, or transverse, and we used muscle orientation to group our alleles into phenotypic classes. For a given allele, we identified the muscles that failed to acquire the correct orientation, and further categorized the orientation phenotypes as defects in myotube elongation (round muscles), in muscle attachment site selection, or in inappropriate branching (Table 1). In addition to orientation phenotypes, the myogenic alleles caused individual muscles to be absent from every hemisegment, produced a thin muscle phenotype throughout the embryo and, in rare occasion, produced muscles that were larger than wild-type controls. The phenotypes we observed were not mutually exclusive, so we grouped the alleles by the primary phenotype, which was the most frequent phenotype we observed (Table 1). Our classification strategy produced 6 phenotypic classes: (1) all 5 *slou>tdTomato* expressing muscles showed orientation defects (Figure 2A), (2) LO1/DT1 orientation defects (Figure 2B), (3) VA2/VA3 orientation defects (Figure 2C), (4) orientation defects in 3–4 *slou>tdTomato* expressing muscles (Figure 2D), (5) thin muscles, and (6) missing muscles. We also assigned alleles to a seventh phenotypic class in which the muscle phenotypes were severe and seemingly non-specific, perhaps due to defects in anterior–posterior patterning, germ band retraction, or dorsal closure.

Complementation analysis identified 25 uncharacterized morphogenetic loci

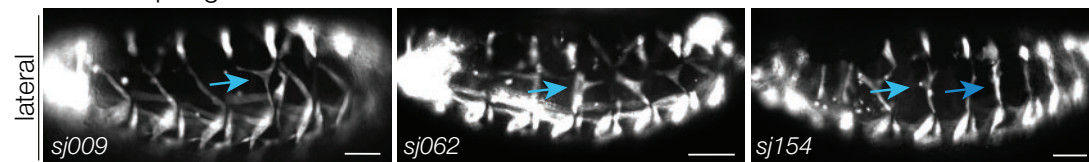
Our phenotypic classes could reflect relative allele strength, so we performed complementation analysis among all 58 alleles, and identified 11 complementation groups with multiple alleles and 33 complementation groups with just a single allele (Table 2). Complementation groups with multiple alleles had representatives from a single phenotypic class (e.g., *sj109* and *sj245*; see Materials and Methods for allele nomenclature) and from multiple phenotypic classes (e.g., *sj264* and *sj455*). These data argue mutations in a single locus can cause overlapping as well as distinct morphogenetic phenotypes. In total, we identified 44 loci that regulate muscle morphogenesis. Alleles in 32 loci appeared to cause specific muscle phenotypes (classes 1–6), and alleles of the remaining 12 loci caused severe, and likely nonspecific, phenotypes (class 7).

To map our myogenic alleles, we first assembled a collection of stocks that carried lethal mutations in known regulators of muscle morphogenesis for complementation analysis. We have characterized 4 genes on the second chromosome that regulate myotube guidance including *hoi polloi* (*hoip*) (Johnson et al. 2013; Williams et al. 2015), *pyramus* (*pyr*) and *thisbe* (*ths*) (Yang et al. 2020b), and *back seat driver* (*bsd*) (Yang et al. 2020a). *kon tiki* (*kon*) (Schnorrer et al. 2007), *slit*, *robo* (Kramer et al. 2001), and *tumbleweed* (*tum*) (Guerin and Kramer 2009; Yang et al. 2020a) direct myotube guidance and are also located on the second chromosome. A previous screen for regulators of muscle morphogenesis on the second chromosome identified *arrow* (*arr*), *barren* (*barr*), *Epidermal growth factor receptor* (*Egfr*), *eyes absent* (*eya*), *patched* (*ptc*), *Regulator of cyclin A1* (*Rca1*), *Star* (*S*), *Sin3a*, *smoothened* (*smo*), *sticks and stones* (*sns*), *teashirt* (*tsh*), and *zipper* (*zip*) (Chen et al. 2008).

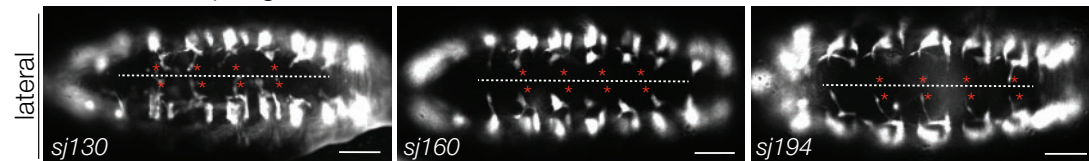
A Morphogenesis defects-5 muscles

slou>tdTomato

B LO1 morphogenesis defects



C VA2/VA3 morphogenesis defects



D LO1/VA2/VA3 morphogenesis defects

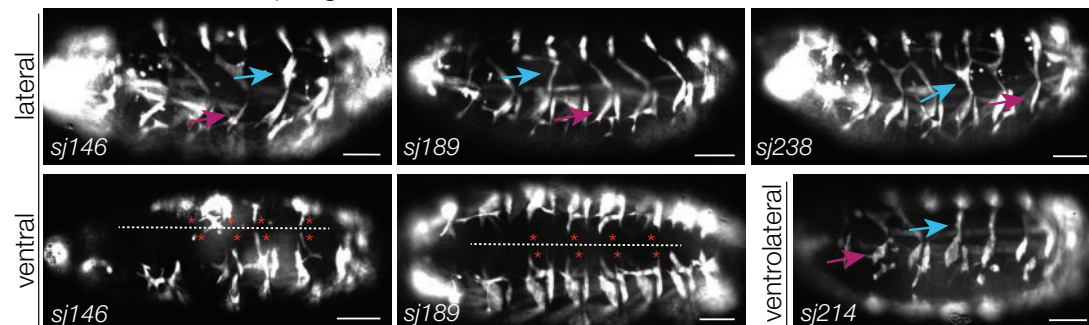


Figure 2 Phenotypic classes. Live Stage 16 embryos that expressed *slou>tdTomato*. In lateral views, LO1 (blue arrows) and VA2 (magenta arrows) muscles are indicated. In ventral views, the ventral midline (dotted line) and the expected positions of VA3 attachment sites (asterisks) are highlighted. (A) The orientation and morphology of all 5 muscles (LO1, DT1, VT1, VA2, and VA3) were affected. (B) LO1 morphogenesis defects. Oblique morphology often transformed to longitudinal morphology (e.g., sj154). (C) VA2/VA3 morphogenesis defects. VA3 muscles frequently failed to attach near the ventral midline (red asterisks). (D) LO1/VA2/VA3 morphogenesis defects. Muscle phenotypes similar to (B, C). Notice VA3 crosses the ventral midline in sj146.

A total of 19 muscle morphogenesis loci have thus been mapped to the second chromosome.

Complementation analysis between our screen alleles and the known regulators of muscle morphogenesis showed that 13 of our mutations were allelic to 6 morphogenetic loci. *sj286* and *sj362* mapped to *bsd*, which encodes a ser/thr kinase (Figure 3A). We Sanger sequenced the *bsd* alleles, and found *bsd^{sj286}* is an A140V missense mutation in the ATP binding pocket and *bsd^{sj362}* is a D590G missense mutation in the kinase domain. Our previous study suggested *bsd* kinase activity is required for myotube guidance (Yang et al. 2020a), and the identification of kinase domain alleles in the current screen argues *bsd* is an essential kinase for muscle morphogenesis.

This is a fibroblast growth factor (FGF) ligand and is required for LO1 morphogenesis and VA3 founder cell fate specification (Yang et al. 2020b). Two of our alleles mapped to *ths*. *ths^{sj102}* and *ths^{sj237}* embryos showed muscle phenotypes consistent with defects in myotube guidance (Figure 3B), and VA3 muscles were missing from some segments in *ths^{sj102}/Df(2R)ths238* and *ths^{sj237}/Df(2R)ths238* transheterozygous embryos (Figure 3B). Overall, *ths^{sj237}* appeared to cause more severe muscle phenotypes than *ths^{sj102}*. This is comprised of an N-terminus FGF signaling domain and an inhibitory C-terminal domain that is cleaved for full signaling activity (Tulin and Stathopoulos 2010). Although we did not sequence the *ths* alleles, it is possible that *ths^{sj102}* and *ths^{sj237}* affect different functional domains of the protein or the ability of *Ths* to be cleaved.

Kon is an orphan transmembrane receptor that directs myotube guidance (Schnorrer et al. 2007), and three of our alleles mapped to *kon*. *kon^{sj11}* and *kon^{sj204}* caused some of the strongest phenotypes in our screen, whereas *kon^{sj525}* embryos showed more modest phenotypes (Figure 3C). *Tum* is a GTPase activating protein that directs microtubule reorganization during myotube guidance (Guerin and Kramer 2009), and one of our alleles mapped to *tum* (*tum^{sj316}*, Table 1). We also identified new alleles in *barr*, *ptc*, and *sns*, which were identified in a previous muscle morphogenesis screen (Chen et al. 2008).

Surprisingly, we did not recover alleles in *slit* or *robo*, which are known regulators of myotube guidance (Kramer et al. 2001), or in *hoip*, which encodes an RNA binding protein that is required for myotube guidance (Johnson et al. 2013), which suggests our screen did not completely saturate morphogenetic loci on the second chromosome. However, we recovered 29 alleles in 25 loci that complemented all known regulators of muscle morphogenesis. Thus, 25 muscle morphogenesis genes from our screen remain to be identified.

Salm directs embryonic muscle morphogenesis

Thirty muscles develop in each embryonic hemisegment at a unique position and with a unique morphology. FGF signaling regulates the morphology of just a subset of muscles, presumably due to restricted expression of the FGF ligands *Pyr* and *Ths* (Yang et al. 2020b), and we wanted to identify additional pathways that regulate the morphogenesis of a subset of muscles. LO1 muscles in *sj154* and *sj340* embryos showed a longitudinal orientation instead of an oblique orientation, but the remaining *slow>tdTom* expressing muscles looked normal (Figure 2B). RNA deep sequencing (RNAseq) of *sj154* and *sj340* embryo lysates identified two independent nonsense mutations in *spalt-major* (*salm*), and *salm¹* failed to complement the LO1 muscle phenotype in *sj154* and *sj340* embryos (Figure 4A). *salm* encodes a zing finger transcription factor that controls fiber type identity during adult

myogenesis (Schönbauer et al. 2011; Bryantsev et al. 2012), but a role for *salm* in embryonic muscle morphogenesis has not been characterized. Our data suggest *Salm* could be a transcriptional regulator of myotube guidance.

Epigenetic regulation of myoblast fusion and myotube guidance

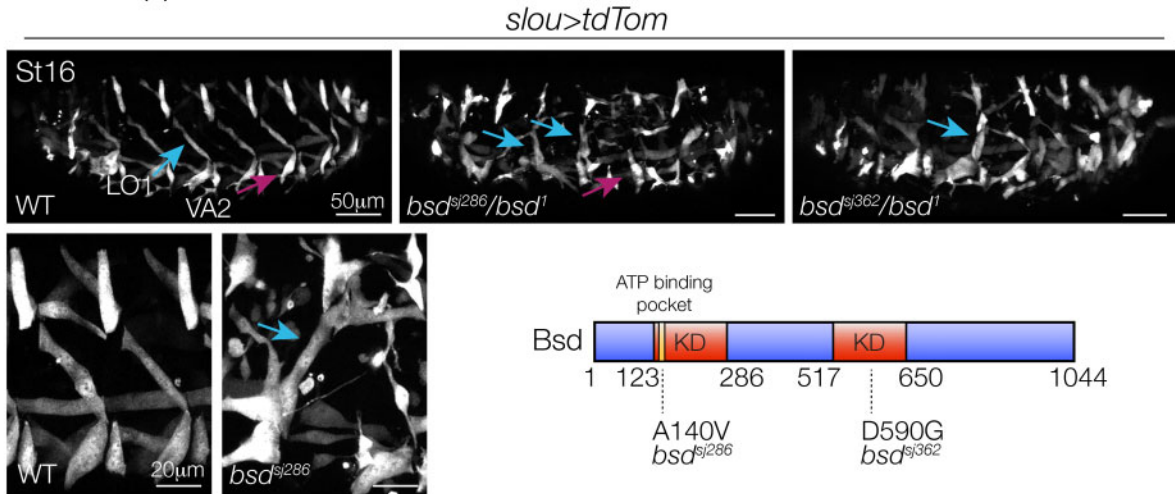
The cellular mechanisms of myoblast fusion and myotube guidance involve cytoskeletal dynamics, so distinguishing fusion phenotypes from guidance phenotypes can be difficult. Our complementation analysis with known regulators of muscle morphogenesis showed *sj266* and *sj440* failed to complement *barr^{L305}*. All 5 *slou>tdTom* expressing muscles showed morphology defects in *barr^{sj266}/barr^{sj440}* embryos (Figure 4B), but *barr^{sj440}* muscles were thin while *barr^{sj266}* muscles were normal size (Figures 2A and 4B). Thin muscles are indicative of myoblast fusion defects, so we assayed myoblast fusion in *barr^{sj440}* embryos. *sj302* and *sj359* embryos also had thin muscles, and these alleles mapped to a known regulator of myoblast fusion *sns*. Each of the 30 embryonic muscles begins development as a founder cell that fuses with neighboring fusion competent myoblasts. The first round of myoblast fusion causes an increase in the number of nuclei that express founder cell markers including the transcription factors *Nautilus* and *Kruppel*, or the transgene *rp298.lacZ*, and founder cell markers have been used to assay myoblast fusion in Stage 12 embryos (Chen and Olson 2001; Chen et al. 2003; Johnson et al. 2013). The number of *rp298.lacZ* nuclei in Stage 12 *barr^{sj440}* embryos was less than control embryos and largely equivalent to *sns^{sj302}* embryos (Figure 4C). At the end of embryogenesis, the number of myonuclei per muscle was also reduced in *barr^{sj440}* and *sns^{sj302}* embryos compared to controls (Figure 4C). These data argue that *Barr* regulates myoblast fusion and myotube guidance, and highlight the exciting possibility that the *barr^{sj266}* and *barr^{sj440}* alleles can be used to genetically separate the role of *Barr* in myoblast fusion from its role in myotube guidance.

Although *barr* was identified in a previous muscle screen (Chen et al. 2008), the role of *Barr* during myogenesis is unknown. *Barr* is a chromatin binding protein and is part of the condensin complex that directs chromosome condensation, which is a landmark of early mitosis (Herzog et al. 2013). Because founder cells and fusion competent myoblasts exit the cell cycle prior to myoblast fusion and myotube guidance, it is possible that *Barr* regulates chromatin for a mitotic-independent function during muscle morphogenesis. For example, the Polycomb group proteins repress transcription by binding to specialized cis-regulatory regions, known as polycomb response elements (PREs), and condensing chromatin into a repressed heterochromatic state (Ringrose and Paro, 2007). *Barr* binds to PREs in the *Hox* gene complex and is required for Polycomb-induced gene silencing (Lupo et al. 2001). These data suggest that epigenetic mechanisms regulate myoblast fusion and myotube guidance.

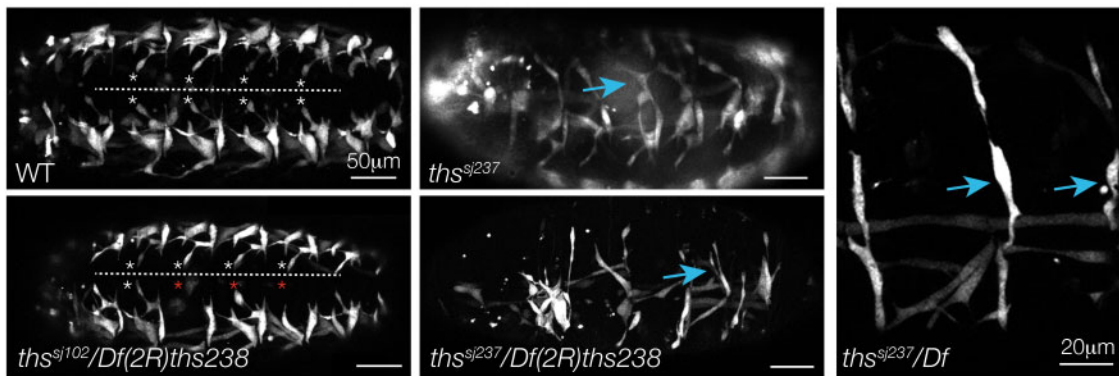
Hh signaling dictates muscle size

The alleles *sj287* and *sj461* produced a rare and unusual phenotype in which the embryonic muscles were larger than wild-type controls, often with the incorrect orientation (Figure 5A). *sj287* and *sj461* complemented all of the alleles in our collection of known regulators of muscle morphogenesis, so we used RNAseq to map the alleles. Surprisingly, *sj287* mapped a W782* nonsense allele in *ptc* and *sj461* mapped to a C313S missense mutation in *ptc*, yet both alleles complemented *ptc^{tuft-D}* in our initial analysis. We extended our complementation analysis and assayed muscle

A Alleles mapped to *bsd*



B Alleles mapped to *ths*



C Alleles mapped to *kon*

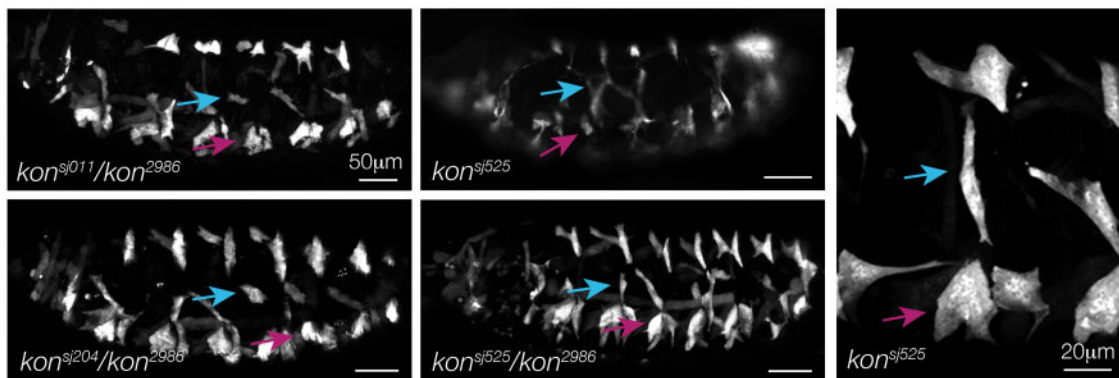


Figure 3 New alleles in known regulators of myotube guidance. Live Stage 16 embryos that expressed *slou>tdTomato*. (A) *bsd^{sj286}* and *bsd^{sj362}* failed to complement *bsd¹*. LO1 muscles (blue arrows) oriented laterally and VA2 muscles (magenta arrows) were rounded or lateral, indicative of myotube guidance defects. A schematic of the *bsd* protein is shown; *bsd^{sj286}* is an A140V missense mutation in the ATP binding domain and *bsd^{sj362}* is a D590G missense mutation in the kinase domain (KD). (B) *ths^{sj102}* and *ths^{sj237}* failed to complement *Df(2R)ths238*. In ventral views, the ventral midline (dotted line) and the expected positions of VA3 attachment sites (asterisks) are highlighted. LO1 muscles often oriented laterally. VA3 muscles were missing or failed attach near the ventral midline (red asterisks). (C) *kon^{sj11}*, *kon^{sj204}*, and *kon^{sj525}* failed to complement *kon²⁹⁸⁶*. LO1 and VA2 muscles were often rounded or laterally positioned. The molecular lesions associated with *ths^{sj102}*, *ths^{sj237}*, *kon^{sj11}*, *kon^{sj204}*, and *kon^{sj525}* were not determined. High and low magnification images are of different embryos.

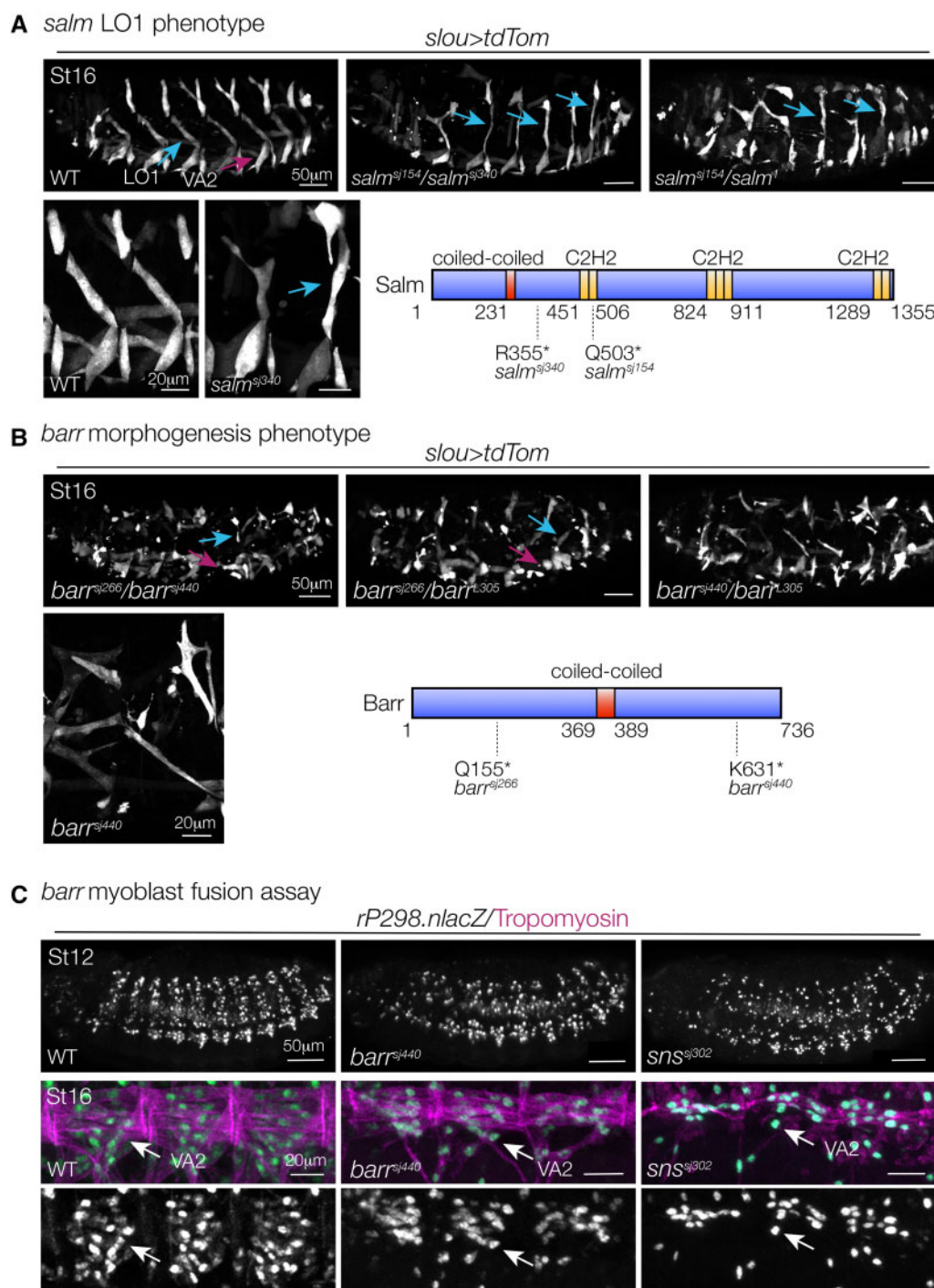


Figure 4 Salm, Barr, and Arr direct muscle morphogenesis. (A–C) Live Stage 16 embryos that expressed *slou>tdTomato* labeled as in Figure 2. (A) *salm^{sj154}* and *salm^{sj340}* failed to complement *salm¹*. Note the longitudinal morphology of LO1 muscles (blue arrows) in transheterozygous and *salm^{sj340}* homozygous embryos. A schematic of the Salm protein is shown. *salm^{sj154}* is a Q503* nonsense mutation; *salm^{sj340}* is a R355* nonsense mutation. Yellow boxes represent the 7 C2H2-type zinc finger domains (C2H2). (B) *barr^{sj266}* and *barr^{sj440}* failed to complement *barr^{L305}*. LO1 (blue arrows) and VA2 (magenta arrows) muscles showed attachment site defects in transheterozygous embryos. *barr^{sj440}* muscles were also thin (high magnification view). A schematic of the Barr protein is shown. *barr^{sj266}* is Q155* nonsense mutation; *barr^{sj440}* is a K631* nonsense mutation. (C) Myoblast fusion assay. Stages 12 and 16 embryos labeled for *rP298.nlacZ* (green) and Tropomyosin (violet). Robust Tropomyosin expression is not detectable until after Stage 12. Stage 12 *barr^{sj440}* and *sns^{sj302}* embryos showed fewer lacZ+ nuclei after the first round of myoblast fusion than control embryos. Stage 16 *barr^{sj440}* and *sns^{sj302}* muscles had fewer myonuclei, particularly the VA2 muscle. High and low magnification images are of different embryos in (A, B).

morphogenesis in embryos transheterozygous for *Df(2R)Exel7098* which uncovers *ptc*. *ptc^{sj287}/Df(2R)Exel7098* and *ptc^{sj461}/Df(2R)Exel7098* embryos phenocopied *sj287* and *sj461* embryos (Figure 5A), confirming the *ptc* coding region mutations are causative of muscle morphogenesis phenotypes.

The mechanisms that regulate muscle size in neonatal, adolescent, and adult vertebrates have been studied in great detail (Sartori et al. 2021). What is less appreciated is that muscle size must also be regulated in the developing embryo, and those unknown mechanisms are in place to limit muscle overgrowth. To our knowledge, the *ptc^{sj287}* and *ptc^{sj461}* embryos are the first examples of oversized embryonic muscles, and these tools may provide a starting point for understanding how muscle size is limited during development.

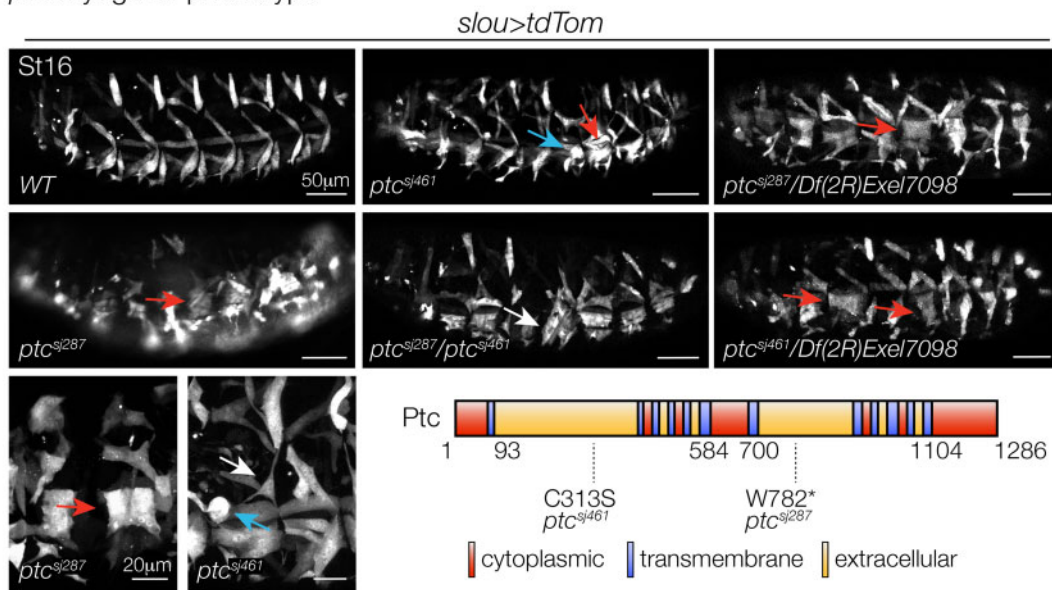
In vertebrates, Hh signaling promotes myoblast differentiation in the somite and myoblast migration in the limb (Münsterberg et al. 1995; Hu et al. 2012). In *Drosophila*, Hh signaling patterns the visceral mesoderm that gives rise to smooth muscle (Bilder and Scott 1998), but the only body wall muscle known to require Hh signaling for proper development is the segment border muscle (SBM) (Jagla et al. 1998). The SBM is not one of the *slou>tdTom* expressing muscles, but

the proximity of the SBM to tendon cells suggests Hh may play a role in attachment site selection at the segment boundary. Consistent with this hypothesis, *ptc^{sj287}* and *ptc^{sj461}* myotubes showed phenotypes consistent with myotube guidance defects (Figure 5A).

Toward a molecular understanding of muscle topography

Our working hypothesis is that muscle topography is established through the actions of short-range secreted signals that provide navigational cues to growing myotubes, and tenocyte expressed cell recognition molecules that direct myotubes to select the correct muscle attachment site. The results from this screen warrant further investigation into Hh signals as navigational cues, and provide new clues into the gene regulatory events, controlled by Salm and Barr, that coordinate cellular guidance and attachment site selection. We successfully used RNAseq to map 6 new alleles without laborious recombination mapping, which brought the total mapped alleles from our screen to 18. However, the mapped alleles represent just a fraction of the mutations with specific phenotypes that we recovered (Figure 5B). Continued

A *ptc* myogenic phenotype



B Screen summary

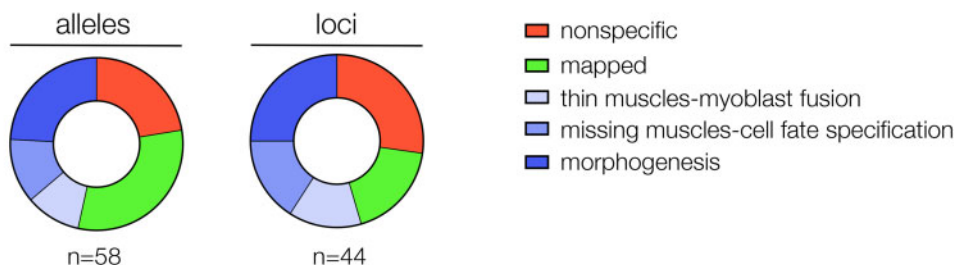


Figure 5 Hh signaling regulates muscle size. (A) Live Stage 16 embryos that expressed *slou>tdTomato*. *ptc^{sj287}/ptc^{sj461}* transheterozygous embryos phenocopied *ptc^{sj287}/Df(2R)Exel7098* and *ptc^{sj461}/Df(2R)Exel7098* embryos. Muscles in *ptc^{sj287}* and *ptc^{sj461}* embryos were oversized, (particularly VA2, red arrows), rounded (blue arrows), and showed attachment site defects (white arrows). High and low magnification images are of different embryos. A schematic of the Ptc protein is shown. *ptc^{sj461}* is a C313S missense mutation in the first extracellular domain; *ptc^{sj287}* is a nonsense mutation in the fourth extracellular domain. (B) Screen summary. Fifty-eight alleles in 44 loci were identified that affect muscle morphogenesis. Greater than half of the alleles were mapped or found to be nonspecific (e.g., phenotypes consistent anterior–posterior patterning, germ band retraction, and dorsal closure defects). Unmapped alleles with specific phenotypes are shaded blue. Six alleles with thin muscles had myoblast fusion defects; 7 alleles that caused

genetic mapping should identify unknown loci with important roles in regulating myotube elongation and muscle attachment site selection.

Acknowledgments

The authors thank all members of the Johnson and Skeath labs for their encouragement and support. They greatly appreciate the reviewers' suggestions and insights, which strengthened the manuscript.

Funding

A.N.J. was supported by NIH R01AR070299 (NIAMS) and J.B.S. was supported by NIH R01NS036570 (NINDS).

Conflicts of interest

None declared.

Literature cited

- Asburner M, Golic K, Hawley R. 2005. *Drosophila: A Laboratory Handbook*. 2nd ed. Cold Spring Harbor, NY: Cold Spring Harbor Laboratory Press.
- Bate M. 1990. The embryonic development of larval muscles in *Drosophila*. *Development*. 110:791–804.
- Bilder D, Scott MP. 1998. Hedgehog and wingless induce metameric pattern in the *Drosophila* visceral mesoderm. *Dev Biol*. 201:43–56.
- Bryantsev AL, Duong S, Brunetti TM, Chechenova MB, Lovato TL, et al. 2012. Extradenticle and Homothorax control adult muscle fiber identity in *Drosophila*. *Dev Cell*. 23:664–673.
- Chen D, Ahlford A, Schnorrer F, Kalchauer I, Fellner M, et al. 2008. High-resolution, high-throughput SNP mapping in *Drosophila melanogaster*. *Nat Methods*. 5:323–329.
- Chen EH, Olson EN. 2001. Antisocial, an intracellular adaptor protein, is required for myoblast fusion in *Drosophila*. *Developmental Cell*. 1:705–715.
- Chen EH, Pryce BA, Tzeng JA, Gonzalez GA, Olson EN. 2003. Control of myoblast fusion by a guanine nucleotide exchange factor, loner, and its effector ARF6. *Cell*. 114:751–762.
- de Jousineau C, Bataillé L, Jagla T, Jagla K. 2012. Diversification of muscle types in *Drosophila*: upstream and downstream of identity genes. *Curr Topics Dev Biol*. 98:277–301.
- Dobin A, Davis CA, Schlesinger F, Drenkow J, Zaleski C, et al. 2013. STAR: ultrafast universal RNA-seq aligner. *Bioinformatics*. 29:15–21.
- Frommer G, Vorbrüggen G, Pasca G, Jäckle H, Volk T. 1996. Epidermal egr-like zinc finger protein of *Drosophila* participates in myotube guidance. *EMBO J*. 15:1642–1649.
- Guerin CM, Kramer SG. 2009. RacGAP50C directs perinuclear gamma-tubulin localization to organize the uniform microtubule array required for *Drosophila* myotube extension. *Development*. 136:1411–1421.
- Herzog S, Nagarkar Jaiswal S, Urban E, Riemer A, Fischer S, et al. 2013. Functional dissection of the *Drosophila melanogaster* condensin subunit Cap-G reveals its exclusive association with condensin I. *PLoS Genet*. 9:e1003463.
- Hu JK, McGlenn E, Harfe BD, Kardon G, Tabin CJ. 2012. Autonomous and nonautonomous roles of Hedgehog signaling in regulating limb muscle formation. *Genes Dev*. 26:2088–2102.
- Jagla T, Bellard F, Lutz Y, Dretzen G, Bellard M, et al. 1998. Ladybird determines cell fate decisions during diversification of *Drosophila* somatic muscles. *Development*. 125:3699–3708.
- Johnson AN, Mokalled MH, Valera JM, Poss KD, Olson EN. 2013. Post-transcriptional regulation of myotube elongation and myogenesis by Hoi Polloi. *Development*. 140:3645–3656.
- Kadam S, McMahon A, Tzou P, Stathopoulos A. 2009. FGF ligands in *Drosophila* have distinct activities required to support cell migration and differentiation. *Development*. 136:739–747.
- Kramer SG, Kidd T, Simpson JH, Goodman CS. 2001. Switching repulsion to attraction: changing responses to slit during transition in mesoderm migration. *Science*. 292:737–740.
- Li H. 2011. A statistical framework for SNP calling, mutation discovery, association mapping and population genetical parameter estimation from sequencing data. *Bioinformatics*. 27:2987–2993.
- Lupo R, Breiling A, Bianchi ME, Orlando V. 2001. *Drosophila* chromosome condensation proteins Topoisomerase II and Barren Colocalize with Polycomb and maintain Fab-7 PRE silencing. *Mol Cell*. 7:127–136.
- Martin M. 2011. Cutadapt removes adapter sequences from high-throughput sequencing reads. *EMBnet J*. 17:3.
- McLaren W, Gil L, Hunt SE, Riat HS, Ritchie GRS, et al. 2016. The ensembl variant effect predictor. *Genome Biol*. 17:122.
- Münsterberg AE, Kitajewski J, Bumcrot DA, McMahon AP, Lassar AB. 1995. Combinatorial signaling by Sonic hedgehog and Wnt family members induces myogenic bHLH gene expression in the somite. *Genes Dev*. 9:2911–2922.
- Nose A, Isshiki T, Takeichi M. 1998. Regional specification of muscle progenitors in *Drosophila*: the role of the msh homeobox gene. *Development*. 125:215–223.
- Ringrose L, Paro R. 2007. Polycomb/Trithorax response elements and epigenetic memory of cell identity. *Development*. 134:223–232.
- Sartori R, Romanello V, Sandri M. 2021. Mechanisms of muscle atrophy and hypertrophy: implications in health and disease. *Nat Commun*. 12:330.
- Schnorrer F, Kalchauer I, Dickson BJ. 2007. The transmembrane protein Kon-tiki couples to Dgrip to mediate myotube targeting in *Drosophila*. *Dev Cell*. 12:751–766.
- Schönbauer C, Distler J, Jährling N, Radolf M, Dodt H-U, et al. 2011. Spalt mediates an evolutionarily conserved switch to fibrillar muscle fate in insects. *Nature*. 479:406–409.
- Tulin S, Stathopoulos A. 2010. Analysis of Thisbe and Pyramus functional domains reveals evidence for cleavage of *Drosophila* FGFs. *BMC Dev Biol*. 10:83.
- Williams J, Boin NG, Valera JM, Johnson AN. 2015. Noncanonical roles for Tropomyosin during myogenesis. *Development*. 142:3440–3452.
- Yang S, McAdow J, Du Y, Trigg J, Taghert P, et al. 2020a. Spatiotemporal expression of regulatory kinases directs the transition from mitotic growth to cellular morphogenesis. *bioRxiv* 06.16.155333.
- Yang S, Weske A, Du Y, Valera JM, Jones KL, et al. 2020b. FGF signaling directs myotube guidance by regulating Rac activity. *Development*. 147:dev183624.

Communicating editor: A. Bashirullah